An energy-efficient torque-vectoring algorithm for electric vehicles with multiple motors

Mechanical Systems and Signal Processing 128 (2019) 655–673

Contents lists available at ScienceDirect

Mechanical Systems and Signal Processing

journal homepage: www.elsevier.com/locate/ymssp

An energy-efficient torque-vectoring algorithm for electric vehicles with multiple motors

C. Chatzikomis [a], M. Zanchetta [b], P. Gruber [b], A. Sorniotti [b,*], B. Modic [c], T. Motaln [c], L. Blagotinsek [c], G. Gotovac [c]

[a] Roborace, Oxford, United Kingdom
[b] University of Surrey, Guildford, United Kingdom
[c] Elaphe Propulsion Technologies, Ljubljana, Slovenia

ARTICLE INFO

Article history:
Received 28 September 2018
Received in revised form 21 December 2018
Accepted 7 March 2019
Available online 2 May 2019

Keywords:
Electric vehicles
Torque-vectoring
Power losses
Cornering

ABSTRACT

In electric vehicles with multiple motors, the individual wheel torque control, i.e., the so-called torque-vectoring, significantly enhances the cornering response and active safety. Torque-vectoring can also increase energy efficiency, through the appropriate design of the reference understeer characteristic and the calculation of the wheel torque distribution providing the desired total wheel torque and direct yaw moment. To meet the industrial requirements for real vehicle implementation, the energy-efficiency benefits of torque-vectoring should be achieved via controllers characterised by predictable behaviour, ease of tuning and low computational requirements. This paper discusses a novel energy-efficient torque-vectoring algorithm for an electric vehicle with in-wheel motors, which is based on a set of rules deriving from the combined consideration of: i) the experimentally measured electric powertrain efficiency maps; ii) a set of optimisation results from a non-linear quasi-static vehicle model, including the computation of tyre slip power losses; and iii) drivability requirements for comfortable and safe cornering response. With respect to the same electric vehicle with even wheel torque distribution, the simulation results, based on an experimentally validated vehicle dynamics simulation model, show: a) up to 4% power consumption reduction during straight line operation at constant speed; b) >5% average input power saving in steady-state cornering at lateral accelerations >3.5 m/s^2; and c) effective compensation of the yaw rate and sideslip angle oscillations during extreme transient tests.

1. Introduction

A wide literature describes the active safety benefits of torque-vectoring (TV), i.e., the application of a direct yaw moment through a controllable left-to-right wheel torque distribution [1,2]. TV can shape the understeer characteristic, i.e., the dependency between steering wheel angle and lateral acceleration, in steady-state cornering, and increase the yaw damping in transient manoeuvres [3–5]. One of the most effective methods to implement TV is through electric vehicles (EVs) with multiple powertrains, which can have an on-board configuration [5], i.e., the motors are part of the sprung mass, or an in-wheel configuration, i.e., the motors are part of the unsprung mass [6–8].

In case of four electric motors (EMs), because of the actuation redundancy, an infinite number of wheel torque distributions can generate the wheel torque demand imposed by the driver or the automated driving system, and the direct yaw

* Corresponding author at: Centre for Automotive Engineering, University of Surrey, GU2 7HX Guildford, United Kingdom.
E-mail address: a.sorniotti@surrey.ac.uk (A. Sorniotti).

https://doi.org/10.1016/j.ymssp.2019.03.012
0888-3270/

List of symbols

a	front semi-wheelbase
a_x	longitudinal acceleration
a_y	lateral acceleration
a_y^*	maximum lateral acceleration of the linear region of the reference understeer characteristic
$a_{y,max}$	maximum lateral acceleration of the reference understeer characteristic
$a_{y,th,high}$, $a_{y,th,low}$	lateral acceleration thresholds for the progressive activation of the feedforward direct yaw moment contribution
b	rear semi-wheelbase
d_f, d_r	roll centre heights of the front and rear suspensions
e_{a_y}	equivalent lateral acceleration error
$e_{a_y,on}$, $e_{a_y,off}$	activation and deactivation thresholds of the relay based on the equivalent lateral acceleration error
F_{drag}	aerodynamic drag force
$F_{x,i}$	longitudinal force of the i-th tyre in the tyre reference system
$F_{y,i}$	lateral force of the i-th tyre in the tyre reference system
$F_{z,f}$, $F_{z,r}$	vertical loads on the front/rear axles
$F_{z,i}$	vertical load of the i-th tyre
g	gravitational acceleration
h_{CG}	centre of gravity height
$J_{EM,loss}$	cost function based on the powertrain power losses in the optimisation routine using the quasi-static model
$J_{F_x,loss}$	cost function based on the longitudinal tyre slip power losses in the optimisation routine using the quasi-static model
$J_{F_y,loss}$	cost function based on the lateral tyre slip power losses in the optimisation routine using the quasi-static model
$J_{P,tot}$	cost function based on the total inverter input power in the optimisation routine using the quasi-static model
$J_{w,i}$	mass moment of inertia of the i-th wheel (including electric motor) about its rotation axis
J_z	vehicle yaw mass moment of inertia
k	sample time
k_{sw}	parameter for the definition of the look-up table breakpoints
k_{us}	understeer gradient
$K_{\varphi,f}$, $K_{\varphi,r}$	front and rear suspension roll stiffness values
l	wheelbase
m	electric vehicle mass
$M_{y,i}$	rolling resistance torque of the i-th tyre
M_z	direct yaw moment
$M_{z,i}$	self-aligning moment of the i-th tyre
$M_{z,ref}$	reference direct yaw moment
$M_{z,ref,FF}$	feedforward contribution of the reference yaw moment
$M_{z,ref,FF,SS}$	steady-state value of the feedforward contribution of the reference yaw moment
$n_{d,EM}$	number of active powertrains
$P_{EM,loss,i}$	power losses of the i-th electric powertrain
$P_{EM,loss,tot}$	total power losses of the electric powertrains
$P_{EM,res}$	power losses of the electric powertrain for zero torque demand
$P_{F_x,loss}$	longitudinal tyre slip power losses
$P_{F_y,loss}$	lateral tyre slip power losses
P_{tot}	total inverter input power
$P_{tot,Passive}$	total inverter input power for the Passive mode
$P_{tot,TV\ Eco}$	total inverter input power for the TV Eco mode
$P_{tot,TV\ Standard}$	total inverter input power for the TV Standard mode
$P_{wheel,tot}$	total power at the wheels
r	yaw rate
r_{ref}	reference yaw rate
R_w	nominal wheel radius
$R_{w,i}$	rolling radius of the i-th tyre
$R_{w,l,i}$	loaded radius of the i-th tyre
S_{a_y}	activation status of the feedback contribution
$T_{b,i}$	braking torque of the i-th corner
$T_{d,i}$	torque demand of the i-th powertrain
$T_{d,L}$, $T_{d,R}$	torque demands on left and right sides of the EV
$T_{d,tot}$	total torque demand of the EV
$T_{d,tot,max}$	maximum value of the total torque demand of the EV

$T_{sw,EM,1}$, $T_{sw,EM,2}$, $T_{sw,EM,3}$ torque thresholds for powertrain switching
V vehicle speed
$V_{slip,x,i}$ longitudinal slip speed of the i-th tyre
$V_{slip,y,i}$ lateral slip speed of the i-th tyre
$V_{x,i}$ longitudinal speed of the i-th corner
w average track width
w_f, w_r front and rear track widths
$W_{a_y,ref}$ scaling factor for the progressive activation of the feedforward contribution of the reference yaw moment
$W_{T_{sw}}$ look-up table for the computation of the feedforward contribution of the reference yaw moment
x_i distance between the centre of the contact patch of the i-th tyre and the EV centre of gravity along the longitudinal axis of the EV
$x_{LUT,W_{T_{sw}}}$ vector with the breakpoints of the look-up table of $W_{T_{sw}}$
$x_{LUT,\rho_{inner}}$, $x_{LUT,\rho_{outer}}$ vectors with the breakpoints of the look-up tables of ρ_{inner} and ρ_{outer}
y_i distance between the centre of the contact patch of the i-th tyre and the EV centre of gravity along the lateral axis of the EV
$y_{LUT,\rho_{inner}}$, $y_{LUT,\rho_{outer}}$ vectors with the outputs of the look-up tables of ρ_{inner} and ρ_{outer}
$y_{LUT,W_{T_{sw}}}$ vector with the outputs of the look-up table of $W_{T_{sw}}$
β sideslip angle
δ average steering angle of the front wheels
δ_{dyn} dynamic steering angle
δ_i steering angle of the i-th wheel
δ_{kin} kinematic steering angle
$\Delta F_{z,f}$, $\Delta F_{z,r}$ front and rear lateral load transfers
$\Delta P_{\%,Passive,TV\ Eco}$ total inverter input power savings of the TV Eco mode with respect to the Passive mode, in percentage
η_{EM} electric powertrain efficiency
ρ_{inner}, ρ_{outer} front-to-total torque distribution ratios on the inner and outer sides of the EV
ρ_L, ρ_R front-to-total torque distribution ratios on the left and right sides of the EV
σ_i slip ratio of the i-th tyre
φ roll angle
ω_i angular speed of the i-th wheel

moment calculated by the TV controller. Hence, energy efficiency is a possible criterion to optimally distribute the wheel torque levels without significantly modifying the cornering response associated with the direct yaw moment. Many papers present energy-efficient wheel torque control allocation (CA) algorithms, e.g., to minimise motor power losses, or tyre slip power losses, or their combination, based on rules or on-line or off-line optimisation methods. [9–47] are a selection from the literature on the topic.

Most of the previous studies reduce the consumption for an assigned cornering response of the EV. Another opportunity, which has been only preliminarily explored in the literature, is represented by the design of energy-efficient understeer characteristics, which correspond to energy-efficient reference yaw rate and direct yaw moment profiles. These can be implemented through any CA algorithm. According to the experimental study in [48] on a vehicle demonstrator with on-board motors, energy-efficient understeer characteristics can bring energy consumption reductions equivalent to those of energy-efficient CA. The benefits of the two methods can be additive. [49] presents a theoretical framework to minimise the powertrain power losses, in case of four identical EMs with specific hypotheses on the shape of the power loss characteristics as functions of torque demand (see also [19]). The tyre slip power losses are used to select the most efficient state among those minimising the powertrain power losses. However, the resulting algorithm is only preliminarily demonstrated in steady-state cornering and could provoke drivability issues in normal driving conditions.

This study complements the research in [49], with the following novelties:

i. An analysis with an experimentally validated non-linear quasi-static model to determine the optimal understeer characteristics and front-to-rear wheel torque distributions in terms of total power input, powertrain power losses and tyre slip power losses.
ii. A set of rules for the energy-efficient EV operation, including consideration of powertrain and tyre slip power losses.
iii. An energy-efficient TV controller based on ii., that consists of: a) a feedforward direct yaw moment contribution to achieve the optimal reference understeer characteristic in nominal conditions (see i.); b) a feedback direct yaw moment contribution to ensure EV stability in emergency conditions; and c) an energy-efficient CA.

The manuscript is organised as follows. Section 2 presents the case study EV and analyses the power loss characteristics of the electric powertrains. Section 3 discusses the experimentally validated vehicle dynamics simulation model and the quasi-static model, which is used in Section 4 to evaluate the effects of understeer characteristic and torque distribution. Section 5 outlines the energy-efficient TV controller, which is assessed in Section 6 through the dynamic simulation model.

2. Powertrain power losses

2.1. Case study electric vehicle

The case study EV is a sport utility vehicle (SUV) prototype (Fig. 1), derived from the conversion of a production internal combustion engine driven vehicle. The EV demonstrator has four equal in-wheel motors based on permanent magnet synchronous technology, directly connected to the wheels, i.e., direct drive. Each motor has a maximum torque of approx. 1.2 kNm and a maximum traction power of approx. 100 kW. The main EV parameters are reported in Table 1. Fig. 2 is a top view schematic of the EV, indicating the naming and sign conventions, such as the numbering order of the four corners. The yaw rate, r, and yaw moment, M_z, are positive in counter-clockwise direction.

2.2. Power loss characteristics of the individual powertrains

The efficiency map of the individual powertrain in Fig. 3(a) was obtained from experimental measurements in traction/regeneration conditions for different torque demands and speeds on the EM test rig available at the Elaphe facilities. The efficiency data include the electro-magnetic and windage power losses in the EM, the power losses in the inverter, and the mechanical power losses in the wheel hub assembly, e.g., caused by the angular contact bearings and seals. As the EM power loss is the prevailing contribution, the notations use the subscript EM. Moreover, the resistance torque of the freely rotating powertrain was measured as a function of motor speed. Such resistance torque generates the EM power loss at zero torque demand, $P_{EM,res}$, i.e., when the unit is switched off.

Fig. 1. The case study EV demonstrator during an experimental test for model validation.

Table 1
Main EV demonstrator parameters.

Parameter	Value
Vehicle mass	2530 kg
Front semi-wheelbase	1.56 m
Rear semi-wheelbase	1.37 m
Front track width	1.68 m
Rear track width	1.74 m
Front tyres	275/40 R20
Rear tyres	315/35 R20
Powertrains	4 in-wheel electric motors (direct drive)

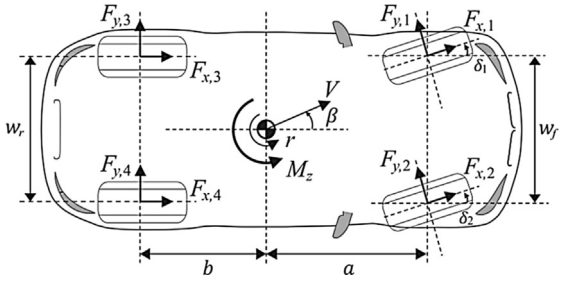

Fig. 2. Schematic top view of the EV with indication of the main parameters and variables.

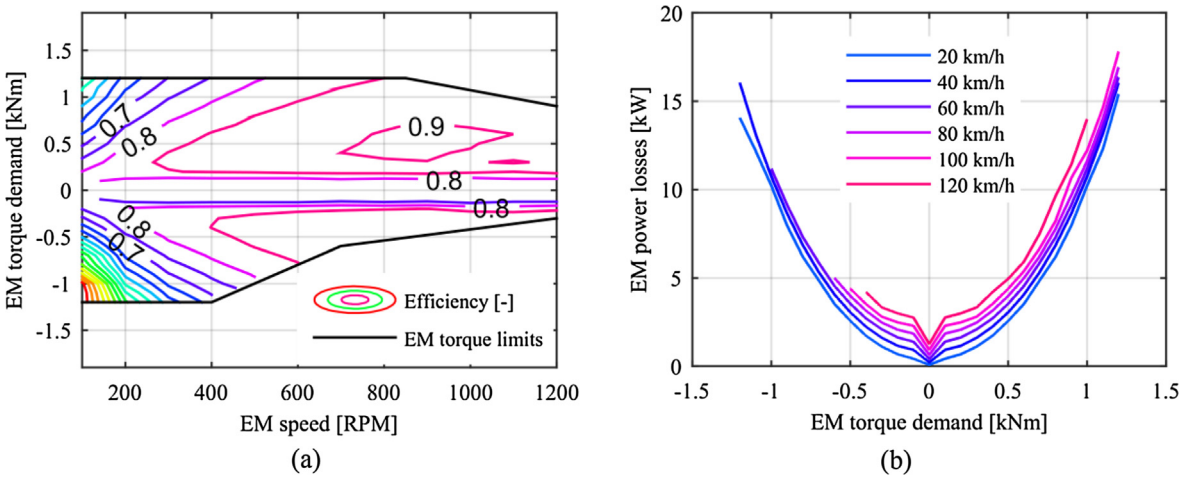

Fig. 3. Experimentally measured (a) efficiency and (b) power loss maps of a single powertrain at different vehicle speeds.

Eq. (1) provides the relationship between power loss and efficiency:

$$P_{EM,loss,i}(T_{d,i},\omega_i)=\begin{cases} T_{d,i}\omega_i\left(\frac{1}{\eta_{EM}(T_{d,i},\omega_i)}-1\right), & T_{d,i}>0 \\ T_{d,i}\omega_i\left(\eta_{EM}(T_{d,i},\omega_i)-1\right), & T_{d,i}<0 \\ P_{EM,res}(\omega_i), & T_{d,i}=0 \end{cases} \tag{1}$$

Fig. 3(b) is the power loss map as a function of torque demand for different vehicle speeds. The power losses are monotonically increasing with a single saddle point, which defines the boundary between a non-convex region at low torque demand, and a convex region at medium-high torque demand. Interestingly, [19,48,49] show that the experimentally measured power loss characteristics of an on-board electric drivetrain, consisting of a high-speed and low-torque EM, single-speed transmission, half-shaft, constant velocity joints and tyre, have similar shape. Hence, Section 2.3 will use the conclusions of the theoretical analyses in [19,49].

2.3. Power loss characteristics of the four electric powertrains

For simplicity of notations, the analyses and formulations of the remainder will focus on positive total wheel torque demands ($T_{d,tot}\geq 0$), i.e., on traction conditions, and the conclusions can be easily extended to the case of $T_{d,tot}<0$. Based on [49], in an EV with multiple EMs with power loss characteristics such as those in Section 2.2, the powertrain power losses are minimised with the progressive activation of an increasing number of EMs with evenly distributed torque, as a function of $T_{d,tot}$.

From the experimentally measured power loss maps of the individual powertrains, Eq. (2) calculates the total powertrain power loss, as a function of the total torque demand, $T_{d,tot}$, vehicle speed, V, and number of active EMs, $n_{d,EM}$:

$$P_{EM,loss,tot}(T_{d,tot},V,n_{d,EM})=\begin{cases} P_{EM,loss,i}\left(T_{d,tot},\frac{V}{R_w}\right)+3P_{EM,loss,i}\left(0,\frac{V}{R_w}\right), n_{d,EM}=1 \\ 2P_{EM,loss,i}\left(\frac{T_{d,tot}}{2},\frac{V}{R_w}\right)+2P_{EM,loss,i}\left(0,\frac{V}{R_w}\right), n_{d,EM}=2 \\ 3P_{EM,loss,i}\left(\frac{T_{d,tot}}{3},\frac{V}{R_w}\right)+P_{EM,loss,i}\left(0,\frac{V}{R_w}\right), n_{d,EM}=3 \\ 4P_{EM,loss,i}\left(\frac{T_{d,tot}}{4},\frac{V}{R_w}\right), \quad n_{d,EM}=4 \end{cases} \tag{2}$$

The results are reported in Fig. 4(a). The close-up of the area of low total torque demand shows the benefit of using a progressively increasing number of powertrains to generate $T_{d,tot}$. In fact, for values of $T_{d,tot}$ lower than a first threshold, defined as $T_{sw,EM,1}$, it is more efficient to generate the total wheel torque with a single EM. Then, for values of torque demand between $T_{sw,EM,1}$ and a second threshold $T_{sw,EM,2}$, and between $T_{sw,EM,2}$ and a third threshold $T_{sw,EM,3}$, it is more efficient to evenly distribute $T_{d,tot}$ among two and three EMs, respectively. Finally, for total torque demands larger than $T_{sw,EM,3}$, the torque should be evenly distributed among the four EMs.

The torque switching points, $T_{sw,EM,1}$, $T_{sw,EM,2}$ and $T_{sw,EM,3}$, are identified from the total power loss calculation for the possible options in terms of number of active EMs. In each of these points, which depend on vehicle speed, a new EM is activated:

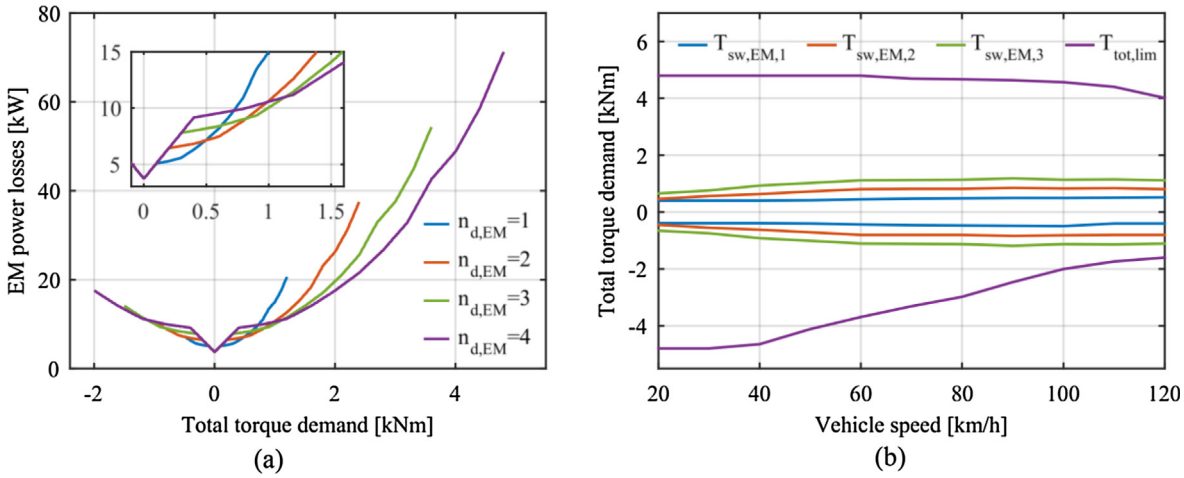

Fig. 4. (a) Total power loss as a function of total torque demand for different numbers of activated EMs, at 100 km/h; and (b) switching torque thresholds for minimising the powertrain power losses, as functions of vehicle speed.

$$min\left(P_{EM,loss,tot}\right) = \begin{cases} P_{EM,loss,tot}\left(T_{d,tot}, V, 1\right), & if \;\; 0 \le T_{d,tot} < T_{sw,EM,1} \\ P_{EM,loss,tot}\left(T_{d,tot}, V, 2\right), & if \;\; T_{sw,EM,1} \le T_{d,tot} < T_{sw,EM,2} \\ P_{EM,loss,tot}\left(T_{d,tot}, V, 3\right), & if \;\; T_{sw,EM,2} \le T_{d,tot} < T_{sw,EM,3} \\ P_{EM,loss,tot}\left(T_{d,tot}, V, 4\right), & if \;\; T_{sw,EM,3} \le T_{d,tot} \end{cases} \tag{3}$$

Fig. 4(b) plots the limits of the torque demand regions for which it is more efficient to use one, two, three or four motors, along with the total torque limits of the four EMs.

2.4. Effect of the direct yaw moment on the powertrain power losses

In an EV with at least two EMs on the same axle, it is possible to generate either a destabilising yaw moment to reduce understeer, or a stabilising yaw moment to increase understeer. The direct yaw moment is provoked by the uneven torque distribution between the two sides of the EV. The torque demands on each side are calculated in Eq. (4) from $T_{d,tot}$ and $M_{z,ref}$, i.e., the direct yaw moment demand, without considering the secondary effects of steering angles and tyre slip ratios.

$$\begin{aligned} T_{d,L} &= 0.5T_{d,tot} - M_{z,ref}\frac{R_w}{w} \\ T_{d,R} &= 0.5T_{d,tot} + M_{z,ref}\frac{R_w}{w} \end{aligned} \tag{4}$$

Assuming for simplicity an even torque distribution between the front and rear motors on each EV side, the total powertrain power losses can be expressed as:

$$P_{EM,loss,tot}\left(T_{d,tot}, M_z, V\right) = 2P_{loss,EM}\left(0.5T_{d,L}, V/R_w\right) + 2P_{loss,EM}\left(0.5T_{d,R}, V/R_w\right) \tag{5}$$

A special case is the generation of $T_{d,tot}$ only by the EMs on one EV side, while zero torque demand is applied to the EMs on the other EV side. In a first approximation, the direct yaw moment for this case is:

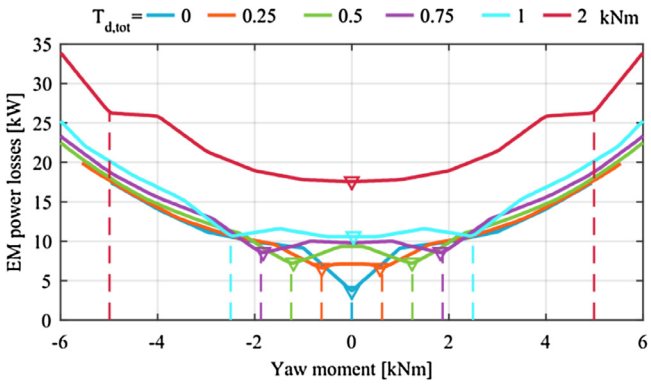

Fig. 5. EM power losses as functions of direct yaw moment for different total torque demands, at 100 km/h (the vertical dashed lines correspond to $M_z = \pm 0.5T_{d,tot}w/R_w$).

$$M_z(T_{d,L}=0, T_{d,R}=T_{d,tot}) = 0.5T_{d,tot}w/R_w$$
$$M_z(T_{d,L}=T_{d,tot}, T_{d,R}=0) = -0.5T_{d,tot}w/R_w \quad (6)$$

Fig. 5 plots the EM power losses as functions of the yaw moment for different torque demands, at V = 100 km/h. The vertical dashed lines indicate the yaw moment values equal to $\pm 0.5T_{d,tot}w/R_w$. For low values of $T_{d,tot}$, such yaw moments correspond to global minima of the total powertrain power loss. At higher values of $T_{d,tot}$, the total power losses are minimized for $M_z = 0$, but the cases with $M_z = \pm 0.5T_{d,tot}w/R_w$ still correspond to local minima. In particular, $P_{EM,loss,tot}$ significantly increases for $|M_z| > 0.5T_{d,tot}w/R_w$, which requires the EMs to operate in traction on one side of the EV and in regeneration on the other side.

3. Electric vehicle models

3.1. Dynamic model

A non-linear 8-degree-of-freedom (8-DOF) vehicle dynamics model was implemented in Matlab-Simulink to assess the performance of the proposed energy-efficient TV controller. The model includes the longitudinal, lateral, yaw and roll dynamics, as well as the rotations of the four wheels. The longitudinal and lateral tyre forces and their interaction are modelled with the Magic Formula (version MF 5.2), coupled with a variable relaxation length formulation of the transient tyre behaviour. The model also considers the suspension elasto-kinematics, the aerodynamic forces and moments, the transient EM response, and the powertrain and tyre power losses (caused by longitudinal and lateral slips, and rolling resistance). The model was validated with experimental measurements on the case study EV in steady-state and transient manoeuvres. For example, Fig. 6 presents the validation results for a 30 m radius skidpad test, which are satisfactory both in terms of cornering response and torque demand/power profiles.

3.2. Quasi-static model

A quasi-static 8-DOF vehicle model (see also [5,50]) was developed to analyse the effect of the non-linear vehicle dynamics on the total power input, powertrain power losses, and longitudinal and lateral tyre slip power losses. The tyre forces, aligning moments and rolling resistance are calculated with the MF 5.2 model. In contrast to the dynamic model (Section 3.1), the time derivatives of the sideslip angle, roll angle and slip ratios are assumed to be zero. This assumption transforms the vehicle model into a system of algebraic conditions that can be solved with a non-linear constraint solver or optimization function, without forward time integration. As a result, the quasi-static model is well-suited for the implementation of optimisation routines for feedforward TV control action design targeting desired understeer characteristics, including conditions of non-zero longitudinal accelerations.

The inputs are the steering angle, δ, total torque demand, $T_{d,tot}$, direct yaw moment demand, $M_{z,ref}$, and front-to-total torque distribution ratios on the left and right sides of the vehicle, ρ_L and ρ_R. The states are the time derivative of the longitudinal vehicle speed, V_{dot}, sideslip angle, β, yaw rate, r, roll angle, φ, and tyre slip ratios, σ_i. The notation "dot" indicates that the time derivatives are algebraic variables. The sideslip angle β is also assumed to be small.

The dynamic steering angle, δ_{dyn}, which is used to define the EV understeer characteristic, is calculated as:

$$\delta_{dyn} = \delta - \delta_{kin} = \delta - \frac{lr}{V} \quad (7)$$

The longitudinal and lateral force balance equations are:

$$m(V_{dot} - rV\beta) = \sum_{i=1}^{4} F_{x,i}\cos\delta_i - \sum_{i=1}^{4} F_{y,i}\sin\delta_i - F_{drag} \quad (8)$$

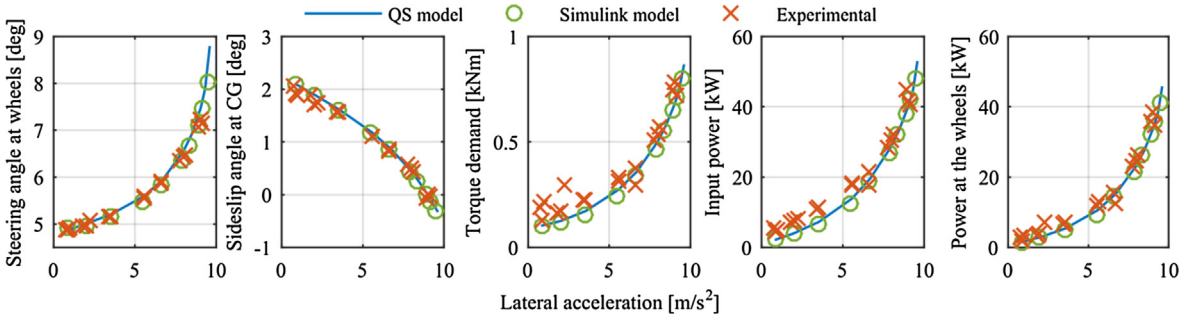

Fig. 6. Experimental validation of the EV simulation models (the 'Simulink model' is the one in Section 3.1, while the 'QS model' is the one in Section 3.2) for a 30 m radius skidpad.

$$m(V_{dot}\beta + rV) = \sum_{i=1}^{4} F_{x,i}\sin\delta_i + \sum_{i=1}^{4} F_{y,i}\cos\delta_i \tag{9}$$

The yaw and roll moment balance equations are:

$$J_z r_{dot} = \sum_{i=1}^{4} F_{x,i}x_i \sin\delta_i + \sum_{i=1}^{4} F_{y,i}x_i \cos\delta_i - \sum_{i=1}^{4} F_{x,i}y_i \cos\delta_i + \sum_{i=1}^{4} F_{y,i}y_i \sin\delta_i + \sum_{i=1}^{4} M_{z,i} \tag{10}$$

$$m(V_{dot}\beta + rV)(h_{CG} - d_f)\cos\varphi + mg(h_{CG} - d_f)\sin\varphi - \left(\sum_{i=3}^{4} F_{x,i}\sin\delta_i + \sum_{i=3}^{4} F_{y,i}\cos\delta_i\right)(d_r - d_f) = (K_{\varphi,f} + K_{\varphi,r})\varphi \tag{11}$$

The vertical tyre loads are calculated from the vertical load on the respective axle, given by:

$$\begin{aligned} F_{z,f} &= mg\tfrac{b}{l} - m(V_{dot} - rV\beta)\tfrac{h_{CG}}{l} - F_{drag}\tfrac{h_{CG}}{l} \\ F_{z,r} &= mg\tfrac{a}{l} + m(V_{dot} - rV\beta)\tfrac{h_{CG}}{l} + F_{drag}\tfrac{h_{CG}}{l} \end{aligned} \tag{12}$$

The front and rear load transfers associated with the lateral acceleration, $\Delta F_{z,f}$ and $\Delta F_{z,r}$, are:

$$\begin{aligned} \Delta F_{z,f} &= \frac{\left(\sum_{i=1}^{2} F_{x,i}\sin\delta_i + \sum_{i=1}^{2} F_{y,i}\cos\delta_i\right) d_F + K_{\varphi,f}\varphi}{w_f} \\ \Delta F_{z,r} &= \frac{\left(\sum_{i=3}^{4} F_{x,i}\sin\delta_i + \sum_{i=3}^{4} F_{y,i}\cos\delta_i\right) d_R + K_{\varphi,r}\varphi}{w_r} \end{aligned} \tag{13}$$

The vertical tyre loads are based on the combination of Eqs. (12) and (13):

$$\begin{aligned} F_{z,1/2} &= 0.5F_{z,f} \pm \Delta F_{z,f} \\ F_{z,3/4} &= 0.5F_{z,r} \pm \Delta F_{z,r} \end{aligned} \tag{14}$$

where the following inequalities manage the conditions of wheel lift:

$$\begin{aligned} 0 &\le F_{z_{1/2}} \le F_{z,f} \\ 0 &\le F_{z_{3/4}} \le F_{z,r} \end{aligned} \tag{15}$$

The torque balance for the i-th wheel is:

$$T_{d,i} - T_{b,i} - F_{x,i}R_{w,l,i} - M_{y,i} - J_{w,i}\omega_{dot,i} = 0 \tag{16}$$

where the angular wheel acceleration is:

$$\omega_{dot,i} = \frac{V_{x,dot,i}}{R_{w,i}}(\sigma_i + 1) \tag{17}$$

The wheel torques are obtained from the front-to-total distribution ratios on each EV side, $T_{d,L}$ and $T_{d,R}$ (see also Eq. (4)):

$$\begin{aligned} T_{d,1} &= \rho_L T_{d,L} \\ T_{d,2} &= \rho_R T_{d,R} \\ T_{d,3} &= (1 - \rho_L)T_{d,L} \\ T_{d,4} &= (1 - \rho_R)T_{d,R} \end{aligned} \tag{18}$$

The longitudinal tyre slip power losses are calculated as:

$$P_{F_x,loss} = \sum_{i=1}^{4} V_{slip,x,i}F_{x,i} \tag{19}$$

while the lateral tyre slip power losses are given by:

$$P_{F_y,loss} = \sum_{i=1}^{4} V_{slip,y,i}F_{y,i} \tag{20}$$

The total wheel power for this EV layout is equal to the EM power, as there is no transmission:

$$P_{wheel,tot} = \sum_{i=1}^{4} \omega_i T_{d,i} \tag{21}$$

The powertrain power losses are calculated from the maps in Section 2:

$$P_{EM,loss,tot} = \sum_{i=1}^{4} P_{EM,loss,i}(T_{d,i}, \omega_i) \tag{22}$$

Hence, the total input power, i.e., the electric input power to the inverters, is:

$$P_{tot} = P_{wheel,tot} + P_{EM,loss,tot} \tag{23}$$

4. Effect of the reference cornering response and control allocation on the EV power losses

4.1. Effect of the understeer characteristic on the EV power losses at constant speed

The quasi-static model is used to investigate the effect of the understeer characteristic, resulting from the TV control action, on the total input power, powertrain power losses and longitudinal and lateral tyre slip power losses.

A set of understeer characteristics is defined, ranging from neutral steering behaviour to more understeering behaviour than the passive vehicle, according to the formulation in [5,50]:

$$\delta = \begin{cases} k_{us}a_y + \frac{la_y}{V^2}, & if\ a_y < a_y^* \\ k_{us}a_y^* + \left(a_y^* - a_{y,max}\right)k_{us}log\left(\frac{a_y - a_{y,max}}{a_y^* - a_{y,max}}\right) + \frac{la_y}{V^2}, & if\ a_y^* \le a_y \le a_{y,max} \end{cases} \tag{24}$$

An oversteering behaviour is not included in this analysis, since such response is considered unsafe for passenger cars. The quasi-static model is run for V =100 km/h, V_{dot} =0 m/s^2, k_{us} = 0:0.01:0.3 deg s^2/m (i.e., for a total of 30 understeer characteristics), a_y^* = 5 m/s^2, $a_{y,max}$ = 10 m/s^2, and $\rho_L = \rho_R = 0.5$. The understeer characteristic of the passive vehicle, i.e., the vehicle with equal torque levels on all wheels, is approximated with k_{us} = 0.109 deg s^2/m, a_y^* =1.03 m/s^2, and $a_{y,max}$ =10 m/s^2. The steering angle, δ, and lateral acceleration, $a_y = V_{dot}\beta + rV$, are imposed as constraints in the quasi-static model, and the system of equations is solved to determine the operating conditions of the EV, including the total power input and individual power loss contributions. The results are presented in Fig. 7, as isocurves of power increase with respect to the optimal understeer characteristics.

The optimal understeer characteristics are calculated with two methods:

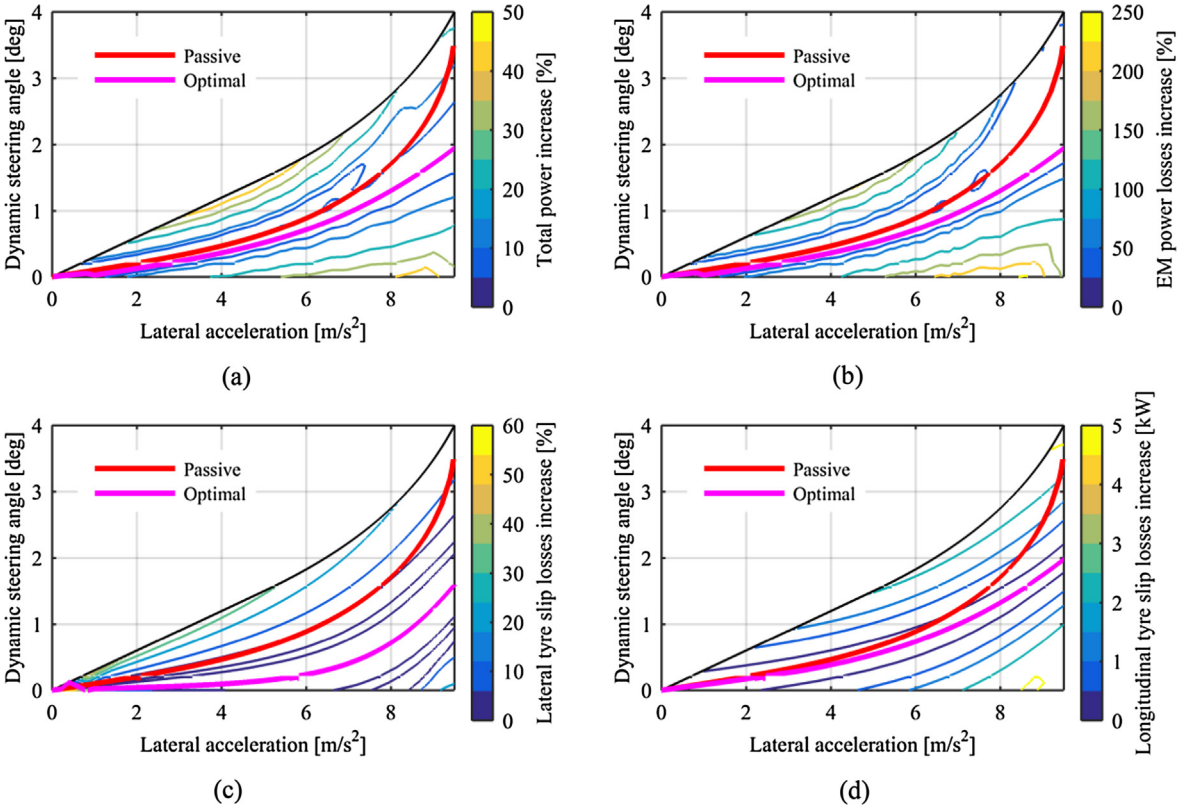

Fig. 7. Variation of a) total power input (in percentage); b) powertrain power losses (in percentage); c) lateral tyre slip power losses (in percentage); and d) longitudinal tyre slip power losses (these are expressed in kW instead of percentage, as the maximum percentage values would be very high and not particularly meaningful), as a function of dynamic steering angle and lateral acceleration, with respect to the optimal understeer characteristic according to the respective cost function. Results are shown for a vehicle speed of 100 km/h.

i. A brute force method, selecting the dynamic steering angle providing the minimum value of the specific cost function among the 30 steering angles available from the sensitivity analysis for the considered lateral acceleration.
ii. Direct optimisation through the Matlab function *fmincon*. In this case, δ is not constrained as it is the optimisation variable.

i. and ii. are used to minimise the following cost functions: a) the total inverter input power, $J_{P,tot} = P_{tot}$; b) the powertrain power losses, $J_{EM,loss} = P_{EM,loss,tot}$; c) the longitudinal tyre slip power losses, $J_{F_x,loss} = P_{F_x,loss}$; and d) the lateral tyre slip power losses, $J_{F_y,loss} = P_{F_y,loss}$. The results of i. and ii. are substantially coincident. Method i. was implemented to verify the results of ii. The remainder of this study will adopt ii., as it does not constrain the dynamic steering angle to be equal to a set of discretized values. Fig. 7 reports the optimal understeer characteristics according to ii., while Fig. 8 plots the corresponding direct yaw moments. Interestingly, for the specific EV and operating conditions, the understeer characteristic that minimises the powertrain power losses corresponds to the direct yaw moment that is achieved for approx. zero torque on the inner side of the EV, i.e., $M_{z,ref} \cong 0.5T_{d,tot}w/R_w$ (see Eq. (6)). As the powertrain power losses are dominant, the understeer characteristic that minimises the total power input is very close to the understeer characteristic minimising the powertrain power losses. The lateral tyre slip power losses are minimised for significantly less understeer, close to a neutral steering behaviour. The average relative decrease of $J_{F_y,loss} = P_{F_y,loss}$ between the passive vehicle and the optimal understeer characteristic is approx. 5%. However, the increased yaw moment and the corresponding larger powertrain power losses make such cornering response inefficient in terms of total input power. The longitudinal tyre slip power losses are minimised for an understeer characteristic that is closer to the optimal one in terms of total input power, with a marginally less understeering behaviour than the passive vehicle.

Fig. 9 investigates the effect of vehicle speed on the optimal understeer characteristic, by minimising $J_{P,tot} = P_{tot}$ at 50 km/h, 75 km/h and 100 km/h. In all cases, the optimal understeer characteristic corresponds to $M_{z,ref} \cong 0.5T_{d,tot}w/R_w$, i.e., with active powertrains only on the outer side of the EV. At low-to-medium lateral accelerations, the total input power reduction with respect to the passive vehicle (see the subplot of the power input change in % and in kW) is more significant at higher speeds.

4.2. Effect of the wheel torque control allocation and total wheel torque demand

Section 4.1 imposed an even front-to-rear torque distribution within each EV side to assess only the effect of the understeer characteristic. To investigate the effect of the front-to-rear torque distribution for a wheel torque applied only to the outer EV side according to the results in Section 4.1, Fig. 10 compares the following cases:

- Even front-to-rear torque distribution (50–50): the torque is evenly distributed between the two wheels on the outer side.
- Rear-wheel-drive (RWD): the torque is applied only to the rear outer wheel.
- The novel CA based on the switching thresholds calculated in Section 2.3 (Switching CA). For low-to-medium lateral accelerations, as the total torque demand at 100 km/h is below $T_{sw,EM,1}$, the torque is applied only to the rear outer wheel. Conversely, for high values of lateral acceleration the total torque demand exceeds $T_{sw,EM,2}$ because of the larger tyre slip power losses, and the torque is evenly distributed between the two outer wheels.

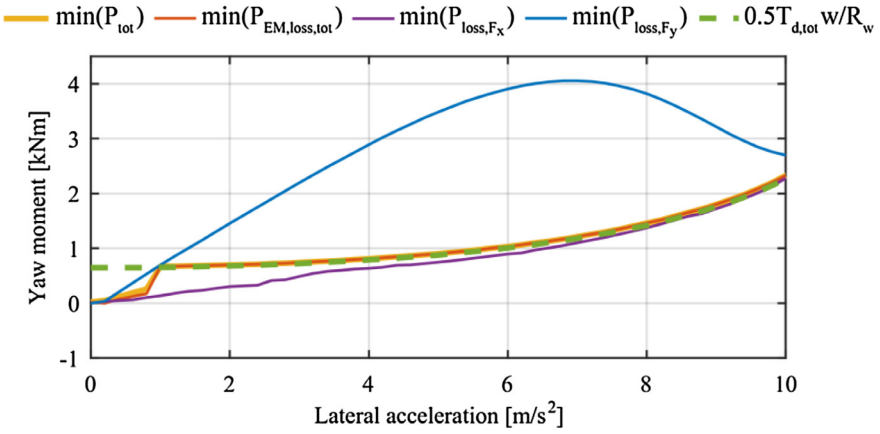

Fig. 8. Direct yaw moments of the optimal understeer characteristics, and direct yaw moment corresponding to zero torque demand on one side of the vehicle (i.e., $0.5T_{d,tot}w/R_w$), as functions of lateral acceleration (vehicle speed of 100 km/h).

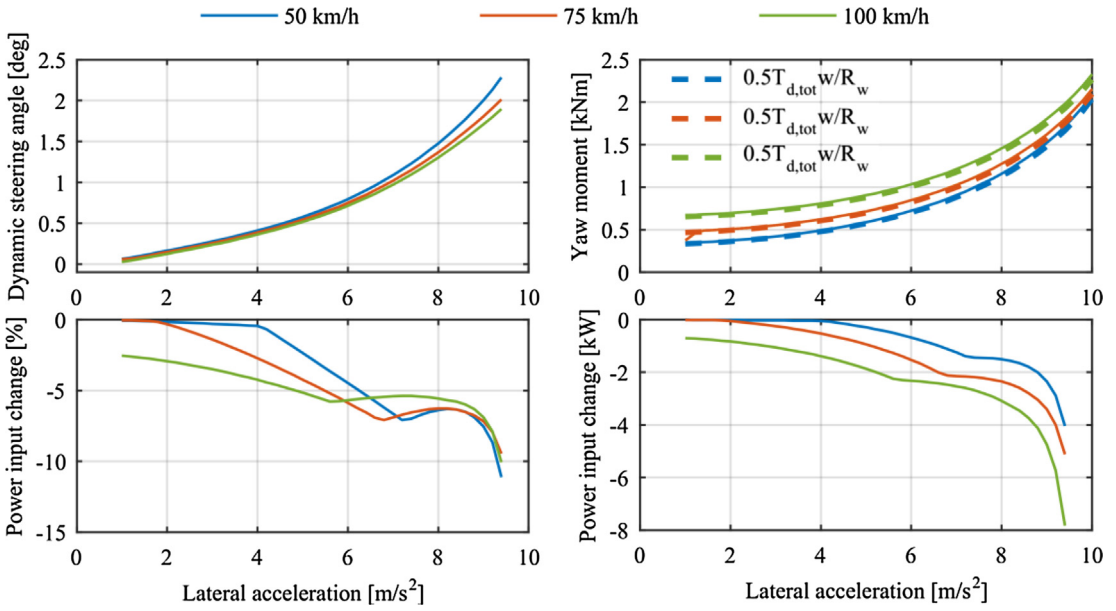

Fig. 9. Results of the input power minimisation for different vehicle speeds with even front-to-total torque distribution within each side of the EV.

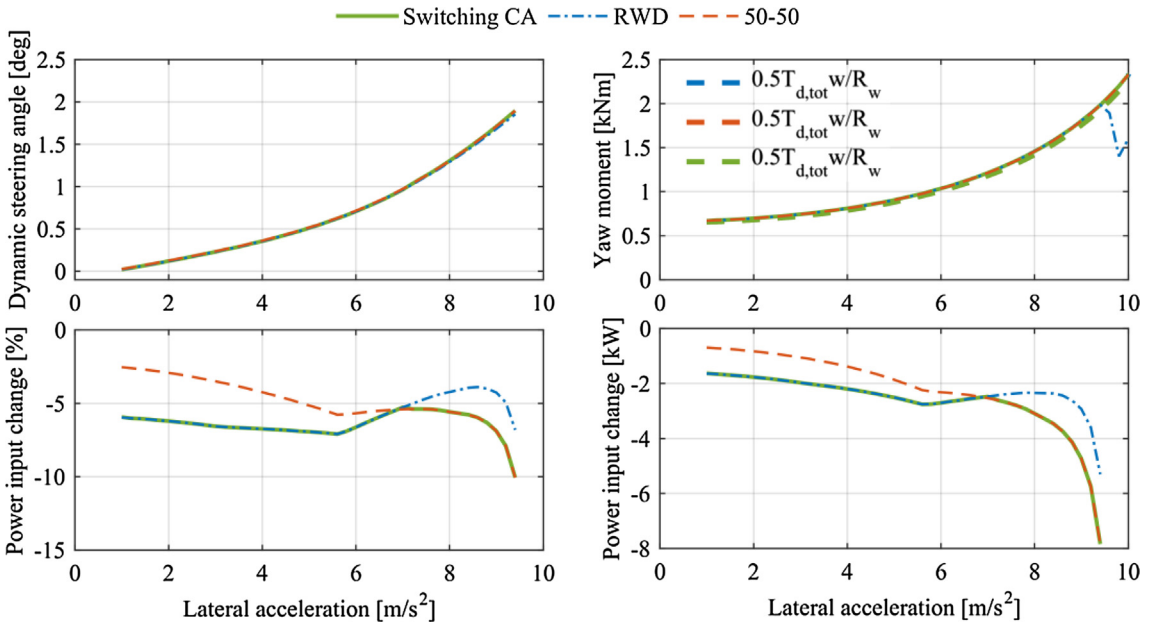

Fig. 10. Results of the input power minimisation for different wheel torque CA strategies at a vehicle speed of 100 km/h.

In Fig. 10 the subplot of the input power change with respect to the passive vehicle shows that the Switching CA combines the low input power of the RWD case for low-to-medium lateral accelerations, with the consumption benefits of the 50–50 case for lateral accelerations larger than 7 m/s^2, thus validating the Switching CA concept. The comparison of the change in input power relative to the passive vehicle in Figs. 9 and 10 shows that the design of energy-efficient understeer characteristic, and thus reference yaw rate and direct yaw moment, can bring larger consumption reductions in cornering than the conventional energy-efficient TV algorithms from the literature (for example, see [16,19]), based only on the CA layer. Moreover, Fig. 10 confirms that the benefits of the energy-efficient reference cornering response and CA are additive.

Figs. 7–10 were obtained for an imposed speed and zero longitudinal acceleration, which implies relatively low levels of $T_{d,tot}$. In Fig. 11 the total torque demand of the quasi-static model is set to constant values, i.e., 450 Nm, 800 Nm, 1100 Nm and 2400 Nm; hence, the longitudinal acceleration varies with the lateral acceleration. The selected values of $T_{d,tot}$

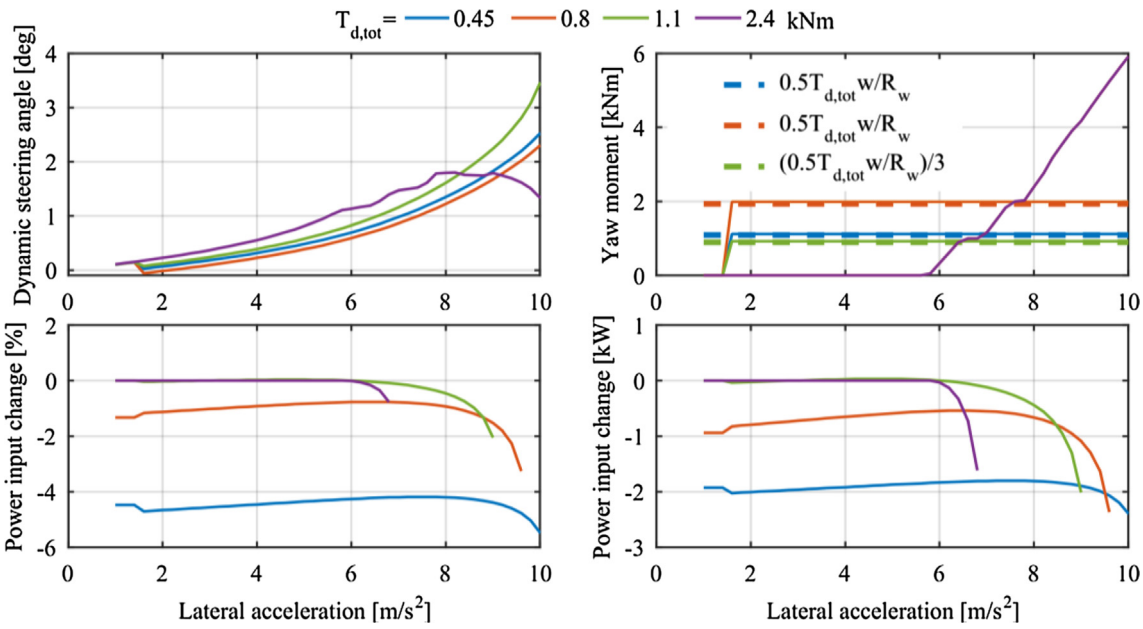

Fig. 11. Results of the input power minimisation at different torque demands with the Switching CA within each side of the EV (vehicle speed of 100 km/h).

correspond to the different operational regions, with progressively increasing number of active EMs, defined by the switching thresholds in Fig. 4(b). The optimisation outputs the dynamic steering angle and direct yaw moment that minimise the total input power for the assigned total torque demand and lateral acceleration, while using the Switching CA within each side of the EV. The results show that:

- For $T_{d,tot} = 450$ Nm, which is lower than $T_{sw,EM,1}$, only the outer rear EM is used (the torque demand of the other drivetrains is negligible) and the optimal yaw moment is $M_{z,ref} \cong 0.5T_{d,tot}w/R_w$, which is consistent with the results in Section 2.3. This is evident from the comparison of the relevant continuous line (optimisation result with the quasi-static model) and dashed line (corresponding to $0.5T_{d,tot}w/R_w$) in the direct yaw moment diagram of Fig. 11. For this torque demand level and the following one, the optimisation prescribes to use only powertrains on the outer side of the EV. The correct number of active EMs minimises the powertrain power losses, while the location of the active powertrains specified by the optimisation routine also accounts for the other sources of power loss, such as the tyre slip power losses, which are generally reduced by a decrease of the level of understeer (see also Fig. 7).
- For $T_{d,tot} = 800$ Nm, which is between $T_{sw,EM,1}$ and $T_{sw,EM,2}$, the torque is evenly distributed between the two outer EMs, and the optimal yaw moment is $M_{z,ref} \cong 0.5T_{d,tot}w/R_w$.
- For $T_{d,tot} = 1100$ Nm, which is between $T_{sw,EM,2}$ and $T_{sw,EM,3}$, the torque is evenly distributed among the two outer motors and the inner rear motor. This result agrees with Section 2.3, prescribing the activation of three EMs, and the optimal yaw moment is $M_{z,ref} \cong T_{d,tot}w/(6R_w)$.
- For $T_{d,tot} = 2400$ Nm, which is greater than $T_{sw,EM,3}$, the optimal yaw moment is about zero up to a lateral acceleration of 6 m/s^2, and the torque is approximately evenly distributed among the four motors, in accordance with Eq. (3). At higher lateral accelerations, the optimal understeer characteristic is progressively less understeering than that of the passive vehicle, and the yaw moment increases (see the relevant continuous line), which represents a deviation from the Section 2.3 results. This is caused by the significance of the tyre slip power losses for the specific scenario. At this torque level, differently from the TV controlled EV, the passive vehicle cannot exceed a lateral acceleration of 6.8 m/s^2, and is characterised by wheel spinning on the inner front corner due to the high torque and low vertical load. This is the reason why the power input change is calculated only up to such lateral acceleration value for this torque demand.

5. Energy-efficient torque-vectoring control algorithm

5.1. Control structure

The above analyses showed that for the case study EV the EM power losses are dominant, and can be minimised with a rule-based algorithm using the EM switching thresholds, functions of the EV speed. This section proposes a TV control structure according to the optimisation results of Figs. 7(a) and 11. The controller consists of: i) a continuously active feedforward direct yaw moment contribution, providing an energy-efficient cornering response in steady-state conditions, for nominal

system parameters; ii) a feedback direct yaw moment contribution intervening only during safety-critical manoeuvres, similarly to the stability control systems actuating the friction brakes in production passenger cars; and iii) a CA algorithm generating the total wheel torque demand and direct yaw moment from i) and ii) through an energy-efficient wheel torque distribution. The following subsections describe i)–iii).

5.2. Feedforward direct yaw moment contribution

In the novel TV control mode of this study, the steady-state value of the feedforward direct yaw moment contribution is derived from the total torque demand and EM switching torque thresholds:

$$M_{z,ref,FF,SS} = \begin{cases} 0.5sign(\delta) W_{a_y,ref} T_{d,tot} w/R_w, & if \;\; 0 \le T_{d,tot} < T_{sw,EM,2} \\ sign(\delta) W_{a_y,ref} T_{d,tot} w/(6R_w), & if \;\; T_{sw,EM,2} \le T_{d,tot} < T_{sw,EM,3} \\ 0, & if \;\; T_{d,tot} \ge T_{sw,EM,3} \end{cases} \tag{25}$$

The first condition in Eq. (25) covers the region up to the second switching threshold, where the wheel torque is applied only to the outer EV side. The second condition covers the operating region between the second and third switching thresholds, where the wheel torque is generated by the two EMs on the outer EV side and the rear EM on the inner side, with equal torque on the three machines. Finally, the feedforward yaw moment is zero when the total torque demand is larger than the third switching threshold, as all EMs generate the same torque.

The sign of the steering angle in Eq. (25) ensures that the direct yaw moment is destabilising in relation to the steering input, thus making the vehicle less understeering. To avoid generating a yaw moment in straight line and to ensure a progressive activation of the feedforward contribution for low values of a_y, a scaling factor, $W_{a_y,ref}$, is defined as a function of the absolute value of the lateral acceleration reference, calculated as $V|r_{ref}|$:

$$W_{a_y,ref} = \begin{cases} 0, & if \quad V|r_{ref}| < a_{y,th,low} \\ \frac{V|r_{ref}| - a_{y,th,low}}{a_{y,th,high} - a_{y,th,low}}, & if \quad a_{y,th,low} \le V|r_{ref}| \le a_{y,th,high} \\ 1, & if \quad V|r_{ref}| > a_{y,th,high} \end{cases} \tag{26}$$

In the actual implementation of the algorithm, a further mechanism is needed to deal with the discontinuities in Eq. (25) and avoid drivability issues, i.e., yaw rate and longitudinal/lateral acceleration oscillations. Therefore, Eq. (25) is modified to include a further weighting factor, $W_{T_{sw}}$, which is the output of a look-up table, function of $T_{d,tot}$. In formulas:

$$\begin{aligned} M_{z,ref,FF,SS} &= 0.5sign(\delta) W_{a_y,ref} W_{T_{sw}} T_{d,tot} \tfrac{w}{R_w} \\ W_{T_{sw}} &= W_{T_{sw}}(T_{d,tot}) \\ x_{LUT,W_{T_{sw}}} &= \begin{bmatrix} T_{sw,EM,1}(1-k_{sw}) \\ T_{sw,EM,1}(1+k_{sw}) \\ T_{sw,EM,2} - (T_{sw,EM,2} - T_{sw,EM,1})k_{sw} \\ T_{sw,EM,2} + (T_{sw,EM,2} - T_{sw,EM,1})k_{sw} \\ T_{sw,EM,3} - (T_{sw,EM,3} - T_{sw,EM,2})k_{sw} \\ T_{sw,EM,3} + (T_{sw,EM,3} - T_{sw,EM,2})k_{sw} \\ T_{d,tot,max} \end{bmatrix} \\ y_{LUT,W_{T_{sw}}} &= \begin{bmatrix} 1 & 1 & 1 & \frac{1}{3} & \frac{1}{3} & 0 & 0 \end{bmatrix}^T \end{aligned} \tag{27}$$

where $x_{LUT,W_{T_{sw}}}$ and $y_{LUT,W_{T_{sw}}}$ are the $W_{T_{sw}}$ look-up table breakpoints and corresponding outputs. $M_{z,ref,FF,SS}$ from Eq. (27) passes through a first order filter, which generates $M_{z,ref,FF}$.

5.3. Feedback direct yaw moment contribution

As the optimal understeer characteristics are rather close to those of the passive vehicle (see Figs. 7(a) and 11) and the non-intervention band of the feedback contribution is relatively wide, in the results of this study the reference yaw rate for the feedback term of the TV controller is the yaw rate corresponding to the steady-state response of the passive vehicle. Alternatively, systematic experimental tests, dynamic model simulations or quasi-static model results with the activated feedforward contribution can generate the look-up tables of the reference yaw rate as a function of the steering input, vehicle speed and total torque demand.

Through multiplication by vehicle speed, the yaw rate error is transformed into an equivalent lateral acceleration error, e_{a_y}:

$$e_{a_y} = V|r_{ref} - r| \tag{28}$$

$e_{a_y}(t)$ determines the activation status of the feedback contribution, through an on-off relay that is defined according to the following discrete time formulation:

$$S_{a_y}(k) = \begin{cases} 1, & if \quad e_{a_y} > e_{a_y,on} \\ S_{a_y}(k-1), & if \quad e_{a_y,off} \le e_{a_y} \le e_{a_y,on} \\ 0, & if \quad e_{a_y} < e_{a_y,off} \end{cases} \tag{29}$$

where $S_{a_y}(k)$ is the activation status of the relay at the sample time k, and $e_{a_y,on}$ and $e_{a_y,off}$ are the lateral acceleration error thresholds for the activation and deactivation of the feedback contribution. When the output of the relay is 0, the yaw rate error is set to zero, and therefore the feedback term is deactivated. When the output of the switch is 1, the reference yaw rate and the actual yaw rate are set to their real values and the feedback part of the TV controller is activated.

The stability-oriented feedback implementation means that the reference yaw rate is not continuously tracked, unless the yaw rate error becomes significant. In this way, the feedback part of the controller does not intervene in steady-state cornering conditions with nominal EV parameters, but ensures stability in safety-critical situations. In the simulations of Section 6, a proportional integral (PI) controller was used, similar to the set-up in [5]. The sum of the feedback and feedforward yaw moment contributions is subject to appropriate saturation, based on the powertrain limits and estimated tyre-road friction condition.

5.4. Wheel torque control allocation algorithm

The torque on each EV side is calculated with Eq. (4), from the total torque demand and reference direct yaw moment. Then Eq. (18) outputs the four wheel torques starting from the front-to-total distribution ratios, ρ_L and ρ_R, which ensure the progressive activation of the EV drivetrains with the total torque demand, according to the optimisation results of Section 4:

$$\rho_L = \begin{cases} 0, & if \;\; 0 \le T_{d,tot} < T_{sw,EM,1} \\ 0, & if \;\; T_{sw,EM,1} \le T_{d,tot} < T_{sw,EM,3} \;\; and \;\; T_{d,L} \le T_{d,R} \\ 0.5, & if \;\; T_{sw,EM,1} \le T_{d,tot} < T_{sw,EM,3} \;\; and \;\; T_{d,L} > T_{d,R} \\ 0.5, & if \;\; T_{sw,EM,3} \le T_{d,tot} \end{cases}$$

$$\rho_R = \begin{cases} 0, & if \;\; 0 \le T_{d,tot} < T_{sw,EM,1} \\ 0, & if \;\; T_{sw,EM,1} \le T_{d,tot} < T_{sw,EM,3} \;\; and \;\; T_{d,L} > T_{d,R} \\ 0.5, & if \;\; T_{sw,EM,1} \le T_{d,tot} < T_{sw,EM,3} \;\; and \;\; T_{d,L} \le T_{d,R} \\ 0.5, & if \;\; T_{sw,EM,3} \le T_{d,tot} \end{cases} \tag{30}$$

When $0 \le T_{d,tot} < T_{sw,EM,1}$, $\rho_L = \rho_R = 0$, therefore only the rear powertrains are activated, and either one or both motors are working depending on the direct yaw moment demand. For example, if the EV is cornering and $M_{z,ref} = M_{z,ref,FF} \neq 0$, the total torque demand is generated only by the rear outer wheel. When $T_{sw,EM,1} \le T_{d,tot} < T_{sw,EM,2}$, the torque demand is evenly distributed between the outer wheels, while the rear inner wheel can be activated if necessary, depending on the feedback contribution. The same CA output is generated for $T_{sw,EM,2} \le T_{d,tot} < T_{sw,EM,3}$, in which Eq. (25) implies an even distribution of the total torque demand among three wheels. Finally, if $T_{d,tot} \ge T_{sw,EM,3}$ and the EV is in steady-state cornering with $M_{z,ref} = M_{z,ref,FF} = 0$, the torque is evenly distributed among the four wheels, while the feedback contribution can bring a torque difference between the two EV sides, with an even distribution within each side.

Similarly to the feedforward contribution, the actual implementation of the CA strategy requires appropriate smoothening, to prevent drivability issues related to swift wheel torque variations. This is done through look-up tables, with the same approach as in Eq. (27):

$$\begin{gathered} \rho_L = \begin{cases} \rho_{inner}, & if \;\; M_{z,ref,FF} \ge 0 \\ \rho_{outer}, & if \;\; M_{z,ref,FF} < 0 \end{cases}; \quad \rho_R = \begin{cases} \rho_{inner}, & if \;\; M_{z,ref,FF} < 0 \\ \rho_{outer}, & if \;\; M_{z,ref,FF} \ge 0 \end{cases} \\ \rho_{inner} = \rho_{inner}(T_{d,tot}); \quad \rho_{outer} = \rho_{outer}(T_{d,tot}) \\ x_{LUT,\rho_{inner}} = \begin{bmatrix} T_{sw,EM,1}(1-k_{sw}) \\ T_{sw,EM,3} - (T_{sw,EM,3} - T_{sw,EM,2})k_{sw} \\ T_{sw,EM,3} + (T_{sw,EM,3} - T_{sw,EM,2})k_{sw} \\ T_{d,tot,max} \end{bmatrix} \\ y_{LUT,\rho_{inner}} = [0\;0\;0.5\;0.5]^T \\ x_{LUT,\rho_{outer}} = \begin{bmatrix} 0 \\ T_{sw,EM,1}(1-k_{sw}) \\ T_{sw,EM,1}(1+k_{sw}) \\ T_{d,tot,max} \end{bmatrix} \\ y_{LUT,\rho_{outer}} = [0\;0\;0.5\;0.5]^T \end{gathered} \tag{31}$$

It must be noted that:

- The algorithm in Eqs. (30) and (31) is expressed as a function of $T_{d,tot}$. Alternatively, it would have been possible to define a switching threshold within each side of the EV and formulate all conditions with respect to the side torque demand.
- The proposed torque distribution criteria are based on the power loss analysis. In production vehicle implementations, further torque distribution conditions could be introduced, based on the effectiveness of the yaw moment generation on each corner, to enhance the EV operation at the limits of handling. For example, these additional conditions could account for the effects of the steering angles [51–52] and the interactions between the longitudinal and lateral tyre forces [53].

6. Simulation results

6.1. Power consumption reductions

This section discusses the EV power consumption performance through vehicle dynamics simulations with the experimentally validated model of Section 3.1. The following EV modes are compared:

- The EV with even torque distribution among the four wheels, indicated as 'Passive'.
- The EV with a conventional TV controller set-up, indicated as 'TV Standard', including: i) a non-linear feedforward contribution targeting the reduction of the level of vehicle understeer; and ii) a continuously active feedback contribution increasing yaw and sideslip damping, and compensating for parameter variations. The TV Standard set-up is equivalent to the Sport mode in [5]. The front-to-total wheel torque distributions within each EV side are 0.5.
- The EV with the energy-efficient TV algorithm proposed in Section 5, indicated as 'TV Eco' in the remainder.

Table 2 reports: i) the total power consumption for the three modes at constant speed, calculated as the sum of the inverter power inputs, which are the products of input voltage and current; and ii) the power saving, $\Delta P_{\%,Passive,TV\ Eco}$, in percentage, of the TV Eco mode with respect to the Passive mode. As the yaw moment is zero in straight line, the consumption is the same for the Passive and TV Standard modes. The power loss characteristics have a non-convex region at low torque demand, and a convex region at medium-high torque demand, which makes the activation of a single powertrain on each EV side for such relatively moderate torque demands, according to the TV Eco mode, more energy-efficient than the Passive and TV Standard configurations, e.g., by approx. 2% at 100 km/h and 4% at 120 km/h.

Figs. 12 and 13 refer to 60 m and 120 m radius skidpad tests. The understeer characteristics of the TV Eco mode are intermediate between those of the Passive mode and TV Standard mode. The total torque demand crosses $T_{sw,EM,1}$ during the 60 m test (at approx. 8 m/s^2), while it crosses both $T_{sw,EM,1}$ (at approx. 7 m/s^2) and $T_{sw,EM,2}$ (at approx. 9 m/s^2) during the 120 m test. The TV Standard mode is more efficient than the Passive mode only during the 120 m test, while in both tests the TV Eco mode brings a >5% power consumption saving with respect to the Passive mode for lateral accelerations >3.5 m/s^2. The maximum saving of the TV Eco mode with respect to the TV Standard mode is approx. 12% at 6 m/s^2 in the 60 m test, and is >5% for the majority of the lateral acceleration values. These results confirm that the energy efficiency-oriented design of the TV controller brings important energy savings, and thus is worth being implemented.

6.2. Cornering response of the TV Eco mode

Given the power consumption focus of the feedforward yaw moment contribution and wheel torque CA of the TV Eco mode, the benefits of such driving mode could be at the cost of: i) irregular cornering response, e.g., induced by the variations of the reference feedforward yaw moment with lateral acceleration; and ii) compromised active safety during extreme transients, e.g., for swift and high-amplitude steering wheel inputs. Hence, this section further analyses the cornering response of the TV Eco mode.

Fig. 14 reports the results for a ramp steer test at a longitudinal speed of 75 km/h, during which a steering wheel input is applied at a rate of 13.5 deg/s. The yaw rate profile is determined only by the feedforward contribution, as r is always within the non-intervention band of the feedback term, defined by the dashed lines in the yaw rate plot. At the beginning of the test,

Table 2
Power consumption of the three EV modes during straight line constant speed operation, and the power saving (in percentage) of the TV Eco mode.

Speed [km/h] Power consumption/saving	80	100	120
$P_{Tot,Passive} = P_{Tot,TV\ Standard}$ [kW]	17.127	27.029	40.754
$P_{Tot,TV\ Eco}$ [kW]	17.107	26.385	39.051
$\Delta P_{\%,Passive,TV\ Eco}$ [%]	0.12	2.38	4.18

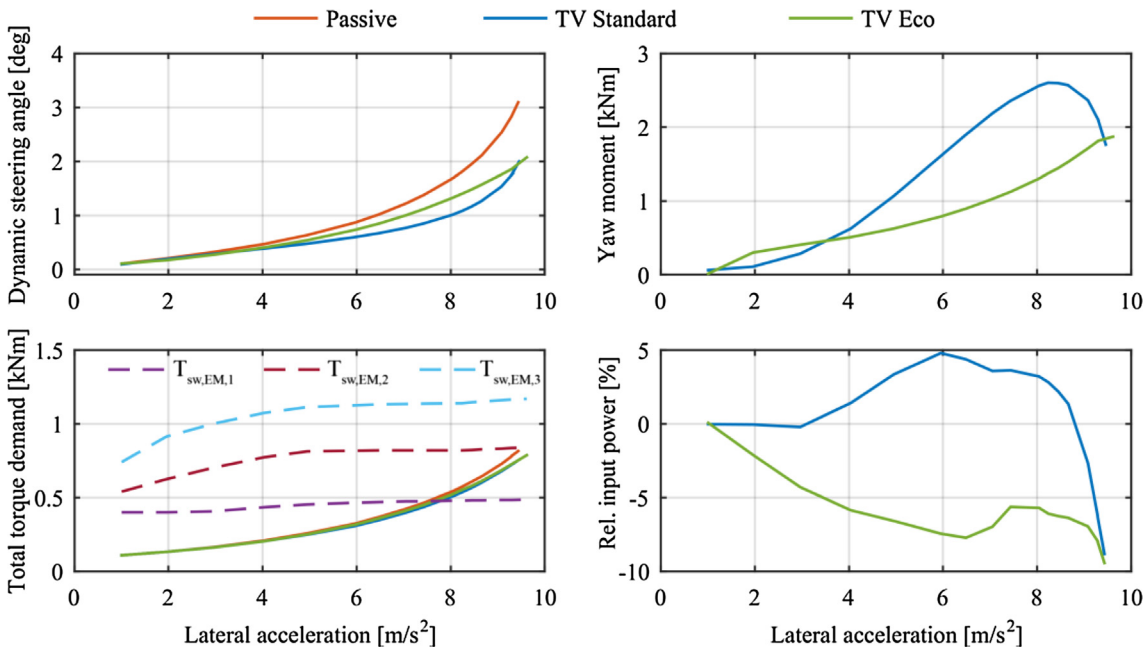

Fig. 12. Comparison of the EV modes during 60 m radius skidpad tests.

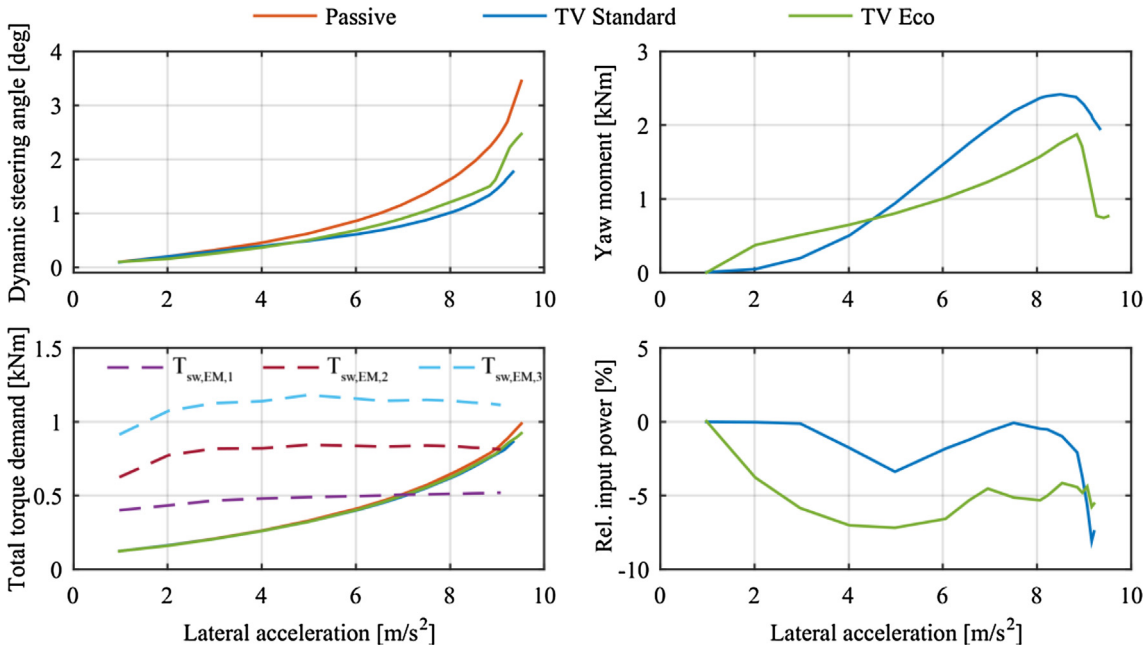

Fig. 13. Comparison of the EV modes during 120 m radius skidpad tests.

for small yaw rate values, $W_{a_y,ref}$ is zero, which prevents the generation of a direct yaw moment, i.e., the traction torque is the same at the two rear powertrains and zero at the two deactivated front powertrains. At approx. 12 s, $W_{a_y,ref}$ progressively increases and the feedforward yaw moment is generated through a traction torque only at the right rear wheel, which is the outer one, i.e., the EV behaves like a single-wheel-drive vehicle, as $T_{d,tot} < T_{sw,EM,1}$. During the steering application, the torque demand progressively increases because of the tyre slip power losses. At approx. 16 s, $T_{d,tot}$ crosses $T_{sw,EM,1}$, and therefore also the front right EM is activated, which is followed by the activations of the left drivetrains. Hence, the direct yaw moment is progressively increasing with lateral acceleration, which enhances the EV responsiveness and 'fun-to-drive',

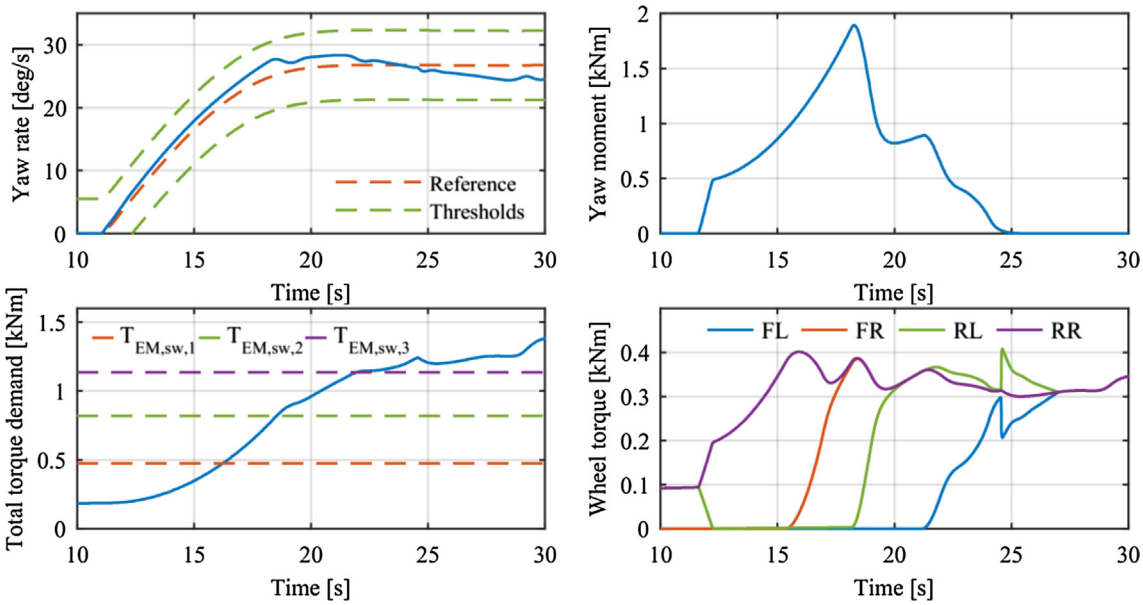

Fig. 14. Ramp steer in the TV Eco mode at 75 km/h (FL: front left; FR: front right; RL: rear left; RR: rear right).

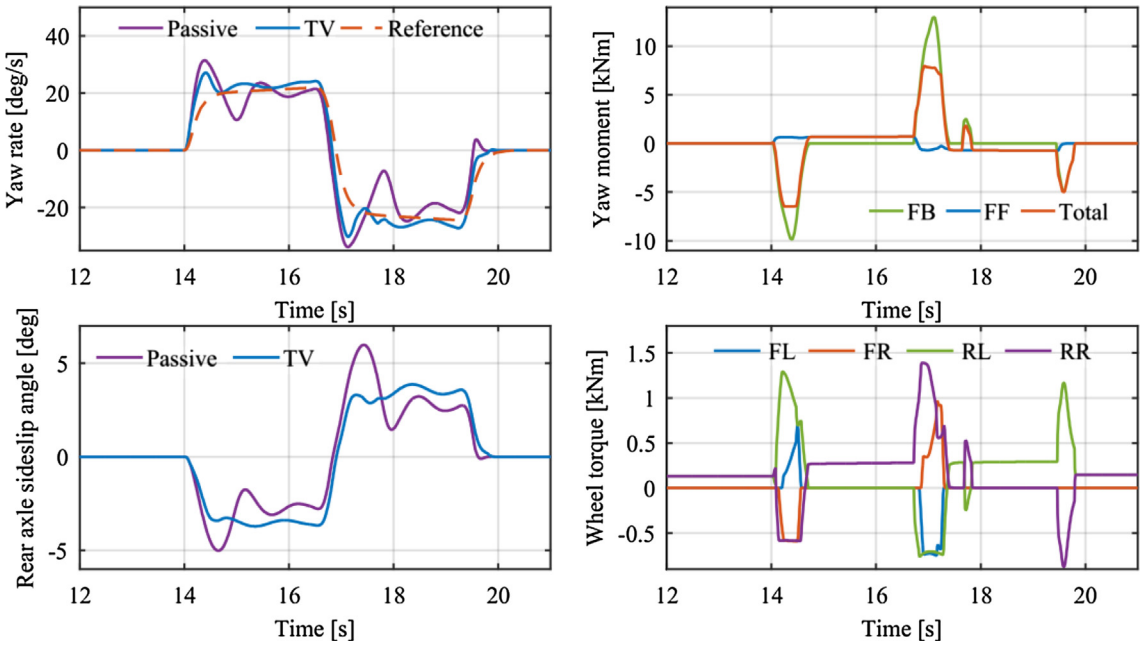

Fig. 15. Double step steer from an initial speed of 100 km/h in the TV Eco mode.

while it decreases to zero at the cornering limit, which ensures EV stability. Despite the developed controller only targets the energy efficiency improvement, such EV cornering behaviour can be considered predictable and safe.

Fig. 15 reports the results of a double step steer test, in which: i) the vehicle is accelerated in a straight line until a speed of 100 km/h is reached; ii) once the speed is stabilised, $T_{d,tot}$ is kept constant; iii) a first steering wheel input is applied at a rate of 400 deg/s, until the steering wheel angle reaches a value of 150 deg, which is then maintained for 2 s; iv) a second steering wheel input is applied at −400 deg/s to reach a value of −150 deg, which is again maintained for 2 s; and v) the driver brings the steering wheel angle back to zero at a rate of 400 deg/s.

In such extreme transients, the TV Eco mode mainly relies on the feedback contribution; in fact, the peaks of the feedback term are several times larger than those of the feedforward term. The actual yaw moment is subject to saturation based on

the powertrain limitations, which determines the difference between its total value and the sum of the feedback and feedforward contributions. With respect to the Passive mode, the TV Eco mode achieves: a) a reduction of the yaw rate peaks after each steering application, i.e., the peak-to-peak distance (between the first overshoot and the first undershoot) is approximately halved; and b) the complete compensation of the rear axle sideslip angle overshoots. The absolute values of the yaw rate in the steady-state phase after each steering transient are marginally higher for the TV Eco mode than for the Passive mode, because of the feedforward contribution, which reduces the level of EV understeer. Overall, the TV Eco mode makes the vehicle not only more reactive but also more stable than the Passive mode, which is the typical and desirable behaviour of a conventional TV controller setup focused on the improvement of the EV cornering response.

7. Conclusions

The analysis of this study leads to the following conclusions:

i. The minimisation of the power losses of the specific in-wheel powertrains implies the progressive switching of an increasing number of electric motors – from one to four – as a function of the total torque demand. The active motors are characterised by an even torque distribution.
ii. The quasi-static model results show that the reduction of the electric powertrain power losses is more important than the reduction of the longitudinal and lateral tyre slip power losses, for most traction and cornering conditions. At constant speed, the understeer characteristics minimising the total input power are marginally less understeering than those of the passive vehicle, while the minimisation of the lateral tyre slip power losses implies a further significant reduction of the understeer level. The appropriate design of the reference understeer characteristics for TV control brings similar or larger energy consumption benefits than the energy-efficient wheel torque control allocation, where the latter is the common implementation of energy-efficient TV in the literature.
iii. A close-to-optimal strategy in terms of total power input can be achieved by activating an increasing number of motors as a function of the total torque demand, with an appropriate switching order (outer rear, outer front, inner rear and inner front) to reduce the tyre slip power losses while minimising the powertrain power losses. The switching thresholds vary with vehicle speed.
iv. A novel TV algorithm was proposed, based on the analytical formulations of: i) the feedforward yaw moment contribution providing an understeer characteristic close to the optimal one in terms of total power input; and ii) the corresponding control allocation strategy. Appropriate smoothening of the feedforward and control allocation terms was presented, to achieve acceptable drivability. A feedback yaw moment contribution that intervenes only for significant values of the yaw rate error provides stability in emergency conditions.
v. The simulation results with a validated vehicle model including the proposed energy-efficient TV algorithm show: i) power consumption reductions of up to 4% during straight line tests at constant speed, with respect to the Passive and TV Standard modes; ii) average power consumption reductions >5% during cornering at lateral accelerations greater than 3.5 m/s^2, compared to the same benchmarks in i); iii) reduced understeer with respect to the Passive mode; and iv) significant improvement of the cornering response during extreme transients with respect to the same EV without TV, caused by the intervention of the feedback contribution.

References

[1] E. Sabbioni, F. Cheli, M. Vignati, S. Melzi, Comparison of torque vectoring control strategies for an IWM vehicle, SAE Int. J. Passenger Cars – Electron. Electr. Syst. 7 (2) (2014) 565–572.
[2] J.W. Griffin, Influences of Drive Torque Distribution on Road Vehicle Handling and Efficiency PhD thesis, University of Nottingham, 2015.
[3] Q. Lu, A. Sorniotti, P. Gruber, J. Theunissen, J. De Smet, H∞ loop shaping for the torque-vectoring control of electric vehicles: theoretical design and experimental assessment, Mechatronics 35 (2016) 32–43.
[4] Q. Lu, P. Gentile, A. Tota, A. Sorniotti, P. Gruber, F. Costamagna, J. De Smet, Enhancing vehicle cornering limit through sideslip and yaw rate control, Mech. Syst. Sig. Process. 75 (2016) 455–472.
[5] L. De Novellis, A. Sorniotti, P. Gruber, J. Orus, J.M.R. Fortun, J. Theunissen, J. De Smet, Direct yaw moment control actuated through electric drivetrains and friction brakes: theoretical design and experimental assessment, Mechatronics 26 (2015) 1–15.
[6] S. Murata, Innovation by in-wheel motor drive unit, Veh. Syst. Dyn. 50 (6) (2012) 807–830.
[7] M. De Santis, S. Agnelli, O. Giannini, Torque vectoring system for improving manoeuvrability of light electric vehicles, AEIT International Annual Conference, 2017.
[8] M. De Santis, S. Agnelli, M. Uras, R. Panciroli, O. Giannini, G. Bella, Carbon fiber-reinforced chassis equipped with four-wheel torque vectoring and steering system, International Conference of Electrical and Electronic Technologies for Automotive, 2018.
[9] J. Brembeck, P. Ritzer, Energy optimal control of an over actuated robotic electric vehicle using enhanced control allocation approaches, IEEE Intelligent Vehicles Symposium, 2012.
[10] Y. Chen, J. Wang, Adaptive energy-efficient control allocation for planar motion control of over-actuated electric ground vehicles, IEEE Trans. Control Syst. Technol. 22 (4) (2014) 1362–1373.
[11] T. Kobayashi, E. Katsuyama, H. Sugiura, E. Ono, M. Yamamoto, Efficient direct yaw moment control: tyre slip power loss minimisation for four-independent wheel drive vehicle, Veh. Syst. Dyn. 56 (5) (2018) 719–733.
[12] S. Bhat, M.M. Davari, M. Nybacka, Study on energy loss due to cornering resistance in over-actuated vehicles using optimal control, SAE Int. J. Veh. Dyn., Stab., NVH 1 (2) (2017) 263–269.
[13] J. Kang, H. Heo, "Control allocation based optimal torque vectoring for 4WD electric vehicle," SAE Technical Paper No. 2012-01-0246, 2012.

[14] B. Li, H. Du, W. Li, B. Zhang, Integrated dynamics control and energy efficiency optimization for overactuated electric vehicles, Asian J. Control 20 (6) (2018) 1–15.
[15] Y. Li, J. Zhang, C. Lv, Y. Yuan, Coordinated control of the steering system and the distributed motors for comprehensive optimization of the dynamics performance and the energy consumption of an electric vehicle, Proc. Inst. Mech. Eng., Part D: J. Automobile Eng. 231 (12) (2017) 1605–1626.
[16] A. Pennycott, L. De Novellis, P. Gruber, A. Sorniotti, T. Goggia, Enhancing the energy efficiency of fully electric vehicles via the minimization of motor power losses, IEEE International Conference on Systems, Man, Cybernetics (SMC), 2013.
[17] Z. Han, X. Nan, H. Chen, Y. Huang, B. Zhao, Energy-efficient control of electric vehicles based on linear quadratic regulator and phase plane analysis, Appl. Energy 213 (2018) 639–657.
[18] S. Koehler, A. Viehl, O. Bringmann, W. Rosenstiel, Energy-efficiency optimization of torque vectoring control for battery electric vehicles, IEEE Intell. Transp. Syst. Mag. 9 (3) (2017) 59–74.
[19] A.M. Dizqah, B. Lenzo, A. Sorniotti, P. Gruber, S. Fallah, J. De Smet, A fast and parametric torque distribution strategy for four-wheel-drive energy-efficient electric vehicles, IEEE Trans. Ind. Electron. 63 (7) (2016) 4367–4376.
[20] A. Wong, D. Kasinathan, A. Khajepour, S.K. Chen, B. Litkouhi, Integrated torque vectoring and power management framework for electric vehicles, Control Eng. Pract. 48 (2016) 22–36.
[21] Y. Suzuki, Y. Kano, M. Abe, A study on tyre force distribution controls for full drive-by-wire electric vehicle, Veh. Syst. Dyn. 52 (sup1) (2014) 235–250.
[22] J. Park, H. Jeong, I.G. Jang, S. Hwang, Torque distribution algorithm for an independently driven electric vehicle using a fuzzy control method, Energies 8 (8) (2015) 8537–8561.
[23] X. Wu, D. Zheng, Contrastive study on torque distribution of distributed drive electric vehicle under different control methods, J. Control Sci. Eng. (2017), Article ID 2494712.
[24] J. Gu, M. Ouyang, D. Lu, J. Li, L. Lu, Energy efficiency optimization of electric vehicle driven by in-wheel motors, Int. J. Automot. Technol. 14 (5) (2013) 763–772.
[25] L. Guo, X. Lin, P. Ge, Y. Qiao, L. Xu, J. Li, Torque distribution for electric vehicle with four in-wheel motors by considering energy optimization and dynamics performance, IEEE Intell. Veh. Symp. (2017).
[26] C.J. Wiet, Energy optimization of an in-wheel-motor electric ground vehicle over a given terrain with considerations of various traffic elements PhD thesis, The Ohio State University, 2014.
[27] A. Goodarzi, M. Mohammadi, Stability enhancement and fuel economy of the 4-wheel-drive hybrid electric vehicles by optimal tyre force distribution, Veh. Syst. Dyn. 52 (4) (2014) 539–561.
[28] X. Zhang, D. Göhlich, X.L. Wu, Optimal torque distribution strategy for a four motorized wheels electric vehicle, Int. Electr. Veh. Symp. Exhibition (EVS28) (2015).
[29] T. Kobayashi, E. Katsuyama, H. Sugiura, E. Ono, M. Yamamoto, "Efficient direct yaw moment control during acceleration and deceleration while turning (first report)," SAE Technical Paper No. 2016-01-1674, 2016.
[30] M.S. Arslan, Vehicle stability enhancement by an energy optimal control approach, in: Intelligent Vehicles Symposium (IV), 2016 IEEE, 2016, pp. 546–551.
[31] T. Kobayashi, E. Katsuyama, H. Sugiura, E. Ono, M. Yamamoto, Direct yaw moment control and power consumption of in-wheel motor vehicle in steady-state turning, Veh. Syst. Dyn. 55 (1) (2017) 104–120.
[32] T. Toshihiro, H. Fujimoto, Proposal of a range extension control system with arbitrary steering for in-wheel motor electric vehicle with four wheel steering, IEEE 13th International Workshop on Advanced Motion Control (AMC), 2014.
[33] R. Wang, Y. Chen, D. Feng, X. Huang, J. Wang, Development and performance characterization of an electric ground vehicle with independently actuated in-wheel motors, J. Power Sources 196 (8) (2011) 3962–3971.
[34] A. Pennycott, L. De Novellis, A. Sabbatini, P. Gruber, A. Sorniotti, Reducing the motor power losses of a four-wheel drive, fully electric vehicle via wheel torque allocation, Proc. Inst. Mech. Eng., Part D: J. Automobile Eng. 228 (7) (2014) 830–839.
[35] X. Yuan, J. Wang, K. Colombage, Torque distribution strategy for a front and rear wheel driven electric vehicle, IEEE Trans. Veh. Technol. 61 (8) (2012) 3365–3374.
[36] S. Sakai, H. Sado, Y. Hori, Dynamic driving/braking force distribution in electric vehicles with independently driven four wheels, Electr. Eng. Jpn. 138 (1) (2002) 79–89.
[37] Z. Wang, C. Qu, L. Zhang, X. Xue, J. Wu, in: Optimal Component Sizing of a Four-wheel Independently-Actuated Electric Vehicle with a Real-time Torque Distribution Strategy, IEEE Access, 2018, pp. 1–16 (in press).
[38] O. Nishiara, S. Higashino, Optimum distribution of lateral and traction/braking forces for energy conservation, IFAC Proc. 46 (21) (2013) 631–636.
[39] H. Fujimoto, S. Harada, Model-based range extension control system for electric vehicles with front and rear driving–braking force distributions, IEEE Trans. Ind. Electron. 62 (5) (2015) 3245–3254.
[40] H. Himeno, E. Katsuyama, T. Kobayashi, "Efficient direct yaw moment control during acceleration and deceleration while turning (second report)," SAE Technical Paper No. 2016-01-1677, 2016.
[41] C. Lin, Z. Xu, Wheel torque distribution of four-wheel-drive electric vehicles based on multi-objective optimization, Energies 8 (5) (2015) 3815–3831.
[42] S. Koehler, A. Viehl, O. Bringmann, W. Rosenstiel, Improved energy efficiency and vehicle dynamics for battery electric vehicles through torque vectoring control, IEEE Intell. Veh. Symp. (2015).
[43] B. Li, A. Goodarzi, A. Khajepour, S. Chen, B. Litkouhi, An optimal torque distribution control strategy for four-independent wheel drive electric vehicles, Veh. Syst. Dyn. 53 (8) (2015) 1172–1189.
[44] K. Ahıska, M.K. Özgören, M.K. Leblebicioğlu, Energy optimal controller for electric vehicles on partially icy roads with heuristic skidding compensation, 15th International Conference on Control, Automation and Systems (ICCAS), 2015.
[45] Y. Chen, J. Wang, Energy-efficient control allocation with applications on planar motion control of electric ground vehicles, American Control Conference (ACC), 2011.
[46] Y. Chen, J. Wang, Fast and global optimal energy-efficient control allocation with applications to over-actuated electric ground vehicles, IEEE Trans. Control Syst. Technol. 20 (5) (2012) 1202–1211.
[47] B. Lenzo, G. De Filippis, A.M. Dizqah, A. Sorniotti, P. Gruber, S. Fallah, W. De Nijs, Torque distribution strategies for energy-efficient electric vehicles with multiple drivetrains, J. Dyn. Syst. Meas. Contr. 139 (12) (2017) 1–13.
[48] G. De Filippis, B. Lenzo, A. Sorniotti, K. Sannen, J. De Smet, P. Gruber, On the energy efficiency of electric vehicles with multiple motors, IEEE Vehicle Power and Propulsion Conference (VPPC), 2016.
[49] G. De Filippis, B. Lenzo, A. Sorniotti, P. Gruber, W. De Nijs, Energy-efficient torque-vectoring control of electric vehicles with multiple drivetrains, IEEE Trans. Veh. Technol. 67 (6) (2018) 4702–4715.
[50] L. De Novellis, A. Sorniotti, P. Gruber, Wheel torque distribution criteria for electric vehicles with torque-vectoring differentials, IEEE Trans. Veh. Technol. 63 (4) (2014) 1593–1602.
[51] F. Bucchi, B. Lenzo, A. Sorniotti, F. Frendo, W. De Nijs, The effect of the front-to-rear wheel torque distribution on vehicle handling: an experimental assessment, 25th International Symposium on Dynamics of Vehicles on Roads and Trucks (IAVSD), 2017.
[52] B. Lenzo, F. Bucchi, A. Sorniotti, F. Frendo, "On the handling performance of a vehicle with different front-to-rear wheel torque distributions," Vehicle System Dynamics (in press). https://doi.org/10.1080/00423114.2018.1546013.
[53] H.B. Pacejka, Tire and Vehicle Dynamics, 3rd Edition., Butterworth-Heinemann, Oxford, 2012.